Influence of Iron Incorporation on the Structural, Optical, and Gas Sensing Properties of Tin Sulfide Nanostructured Thin Films

Tahseen H. Mubarak[1], Hiba Rashid Shakir[2], Fikrat Hikmat Jasim[3], Muhaned Zaidi[4],
Sami Salman Chiad[3] and Yassin Hasan Kadhim[5]
[1]*Department of Physics, College of Science, University of Diyala, 32001 Baqubah, Iraq*
[2]*Department of Optometry, Technical Medical Institute - Al-Mansur, Middle Technical University, 10001 Baghdad, Iraq*
[3]*Department of Physics, College of Education, Mustansiriyah University, 10052 Baghdad, Iraq*
[4]*Department of Medical Physics, Al-Manara College for Medical Sciences, 62001 Amarah, Iraq*
[5]*Department of Optics Techniques, College of Health and Medical Techniques, Al-Mustaqbal University, 51001 Hillah, Iraq*
dr.sami@uomustansiriyah.edu.iq

Keywords: SnS, SPT, Fe Doping, XRD, Bandgap, Gas Sensing, NO_2, Surface Morphology.

Abstract: Iron-doped tin sulfide (SnS:Fe) nanostructured thin films with doping concentrations of 1 and 3 wt% were successfully synthesized using the spray pyrolysis technique (SPT). X-ray diffraction analysis confirmed the formation of polycrystalline films with an orthorhombic crystal structure and a preferred orientation along the (106) plane. The incorporation of Fe enhanced the crystallinity of the films, as evidenced by an increase in crystallite size from 13.56 nm for the undoped sample to 22.78 nm for the 3% Fe-doped film, accompanied by a reduction in dislocation density and microstrain. Atomic force microscopy (AFM) analysis demonstrated that Fe doping significantly improved the surface morphology of the films, resulting in a more homogeneous surface structure. This improvement was evidenced by a reduction in the average particle size from 87.6 nm to 41.1 nm, accompanied by a decrease in surface roughness. Optical studies showed a decrease in the energy bandgap from 1.72 eV to 1.60 eV with increasing Fe content. Gas sensing measurements toward NO_2 at 110 °C indicated that undoped SnS films exhibited the highest sensitivity, while Fe doping reduced performance.

1 INTRODUCTION

Group IV-VI semiconductors are known for their good optoelectronic properties and reduced optical band gaps [1], [2]. SnS has a high absorption coefficient ($\alpha > 10^4$ cm^{-1}) in the visible spectrum [3]. It is less harmful than metal compounds like lead and cadmium [4]-[6]. The components that make up SnS are inexpensive and readily available, and it is chemically stable [7], [8]. The SnS layer structure is orthogonal [9]. The indirect Eg of single-crystal SnS thin films is 1.1 eV, while polycrystalline SnS thin films have a direct energy gap of 1.27–1.5 eV [10]. Tin sulfide has some favourable physical properties that enable its application in solar cells [11], photovoltaics [12], photoconductors [13], and photocatalysis [14], among others. Some methods for preparing SnS films include sputtering [15], vacuum evaporation [16], co-evaporation [17], CBD [18], physical vapor deposition [19], SPT [20], and PLD [21]. Because of its potential, user-friendliness, low initial cost, and the ability to deposit a uniform film over large areas with strict control of composition and thickness, SPT has received much attention [22]-[24]. Iron doping has also emerged as an effective treatment for modifying the inherent physical properties of semiconductor thin films [25]. The incorporation of Fe ions into the SnS crystal lattice can significantly affect the structural characteristics of the films, including crystallinity, grain size, and defect concentration [26]. Moreover, Fe incorporation may introduce localized electronic states within the band gap, thereby modifying the electronic structure and influencing the optical and electrical properties of the material [27]-[29]. We set up this study to investigate how the inclusion of iron affects the structural, optical, and sensing properties of SnS thin films.

2 EXPERIMENTAL

SnS thin films are manufactured using the CSP procedure. The solution was prepared by dissolving 0.1 M $CuCl_2 \cdot 6H_2O$ and thiourea (NH2CSNH2) in 100 mL of redistilled water. The doping agent used was 0.1 M FeCl at 1% and 3% with a base temperature of 400ºC. For the deposition, the following conditions were selected: a spraying rate of 0.15 ml/spray, a spacing of 29 cm between the base of the spraying and the sprayer, a spraying time of up to 8 seconds, an interval of 1.30 minutes between two sprays, and a carrier gas (filtered compressed air) measured at a pressure of 10^5 Pa; thickness was read using gravimetric and was determined to be 300 nm. Transmittance was measured by a UV-Visible spectrophotometer. The alterations in structural properties were examined using XRD. Gas sensitivity in this study was typically evaluated in a cylindrical chamber with a 7.5 cm radius and 15 cm height.

3 RESULTS AND DISCUSSION

The X-ray diffraction (XRD) patterns of pure and Fe-doped SnS thin films are presented in Figure 1. Four dominant diffraction peaks were observed, corresponding to the (008), (106), (110), and (118) crystallographic planes. Among them, the (106) reflection exhibited the highest intensity, indicating that this plane represents the preferred growth orientation of the SnS films. The diffraction peaks are in good agreement with ICDD card No. 39-0354, confirming the successful formation of polycrystalline SnS thin films with an orthorhombic crystal structure.

The structural parameters derived from the XRD data are summarized in Table 1. As the Fe concentration increased from 0 to 3%, the full width at half maximum (FWHM) gradually decreased, indicating improved crystallinity of the deposited films. This reduction in peak broadening was accompanied by an increase in crystallite size from 13.56 to 22.78 nm, suggesting that Fe incorporation promotes grain growth and enhances the structural ordering of the SnS lattice [30]. A corresponding decrease in dislocation density was also observed, with values decreasing from 64.61×10^{14} to 50.60×10^{14} lines/m², indicating a reduction in crystal defects and further confirming the improvement in crystalline quality resulting from Fe doping [31]. Similarly, the microstrain decreased from 29.39×10^{-4} to 25.65×10^{-4} as the Fe concentration increased, reflecting reduced lattice distortion and improved atomic ordering within the crystal structure [32]. The combined changes in crystallite size, dislocation density, and microstrain demonstrate that Fe incorporation significantly enhances the structural quality of SnS thin films. The corresponding structural parameters are listed in Table 1, while Figure 2 illustrates the variation of FWHM, crystallite size, dislocation density, and microstrain with Fe concentration.

Figure 3 presents the atomic force microscopy (AFM) images of pure and Fe-doped SnS nanostructured thin films. The surface morphology reveals a uniform distribution of densely packed grains without visible cracks or voids, indicating the formation of high-quality films. Increasing the Fe concentration resulted in a gradual reduction in the average particle size from 87.6 nm for the undoped film to 61.3 nm and 41.1 nm for the films containing 1% and 3% Fe, respectively. This behavior suggests that Fe doping suppresses grain growth and promotes the formation of finer nanostructures. The surface roughness also decreased with increasing Fe content. The average roughness (Ra) decreased from 9.67 nm to 4.25 nm, while the root-mean-square (RMS) roughness decreased from 8.91 nm to 5.14 nm. These AFM parameters, summarized in Table 2, indicate that Fe incorporation produces smoother and more uniform film surfaces. The observed reduction in particle size and surface roughness can be attributed to changes in the nucleation and surface diffusion processes during thin-film growth [33], [34].

Figure 4 shows the optical transmittance spectra of the pure and Fe-doped SnS thin films. The transmittance in the visible region ranges from 80.6% to 85.5%, indicating good optical transparency. In addition, the transmittance increases toward longer wavelengths, suggesting reduced optical absorption in the near-infrared region [35], [36]. This behavior demonstrates that Fe-doped SnS thin films possess favorable optical properties for potential optoelectronic applications.

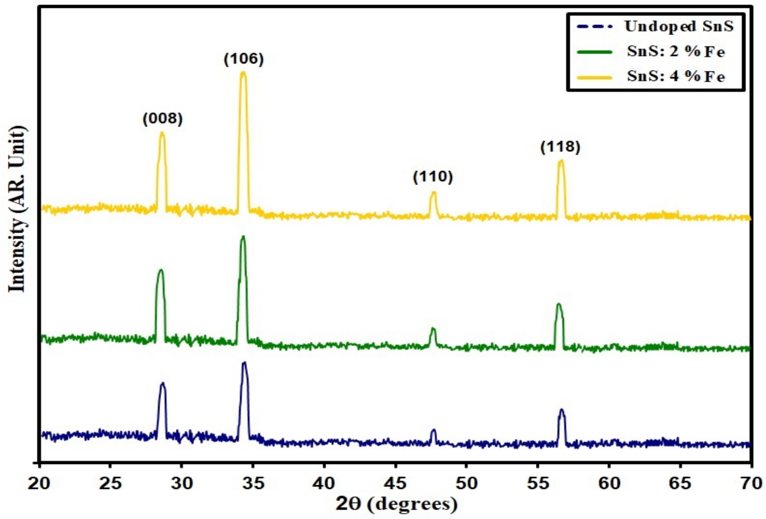

Figure 1: X-ray diffraction (XRD) patterns of pure and Fe-doped SnS thin films.

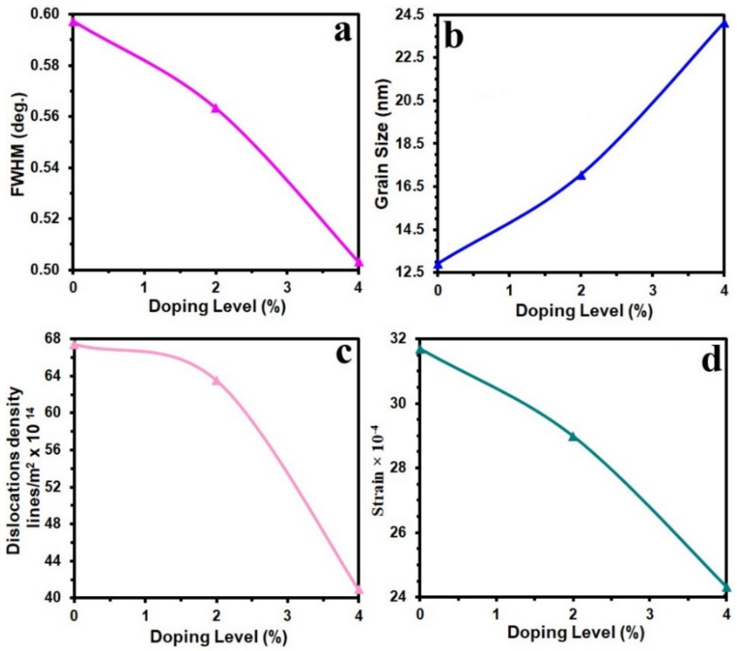

Figure 2: Variation of the structural parameters of pure and Fe-doped SnS thin films: a) full width at half maximum (FWHM), b) crystallite size (D), c) dislocation density (δ), and d) microstrain (ε).

Table 1: D, E_g, and structural coefficient of the SnS and SnS: Fe film.

Specimen	(hkl) Plane	2 θ(°)	FWHM(°)	E_g (eV)	D (nm)	$\delta \times 10^{14}$ (lines/m^2)	$\varepsilon \times 10^{-4}$
Undoped SnS	106	34.28	0.62	1.72	13.56	64.61	29.39
SnS: 2% Fe	106	34.25	0.57	1.65	18.78	57.31	27.63
SnS: 4% Fe	106	34.21	0.52	1.60	22.78	50.60	25.65

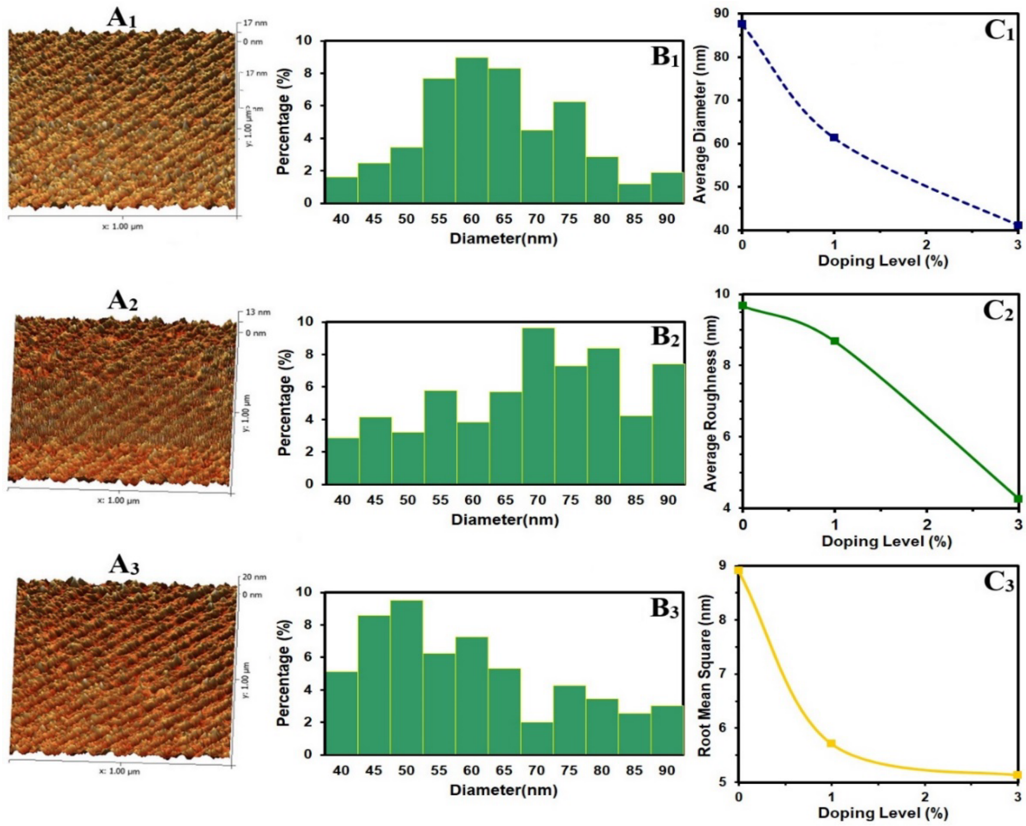

Figure 3: Atomic force microscopy (AFM) surface images of pure and Fe-doped SnS thin films.

Table 2: P_{AFM} of the deposit films.

Samples	P_{av} nm	R_a (nm)	RMS (nm)
Undoped SnS	87.6	9.67	8.91
SnS: 2% Fe	61.3	8.68	5.72
SnS: 4% Fe	41.1	4.25	5.14

Figure 5 shows the optical absorbance spectra of pure and Fe-doped SnS thin films. The absorbance increases with increasing Fe concentration, with the 2% and 4% Fe-doped films exhibiting higher absorbance than the undoped SnS film. This enhancement can be attributed to the increased Fe content, which promotes stronger optical absorption within the films [38], [39].

Figure 6 presents the absorption coefficient spectra of the pure and Fe-doped SnS thin films. The absorption coefficient increases with increasing Fe concentration, indicating enhanced optical absorption after Fe incorporation. A pronounced increase is observed near the absorption edge, followed by a gradual decrease at higher photon energies. The high absorption coefficient values suggest efficient photon absorption and direct electronic transitions within the films. The enhancement in optical absorption with increasing Fe content is attributed to defect-state formation and doping-induced modifications of the electronic structure [42], [43].

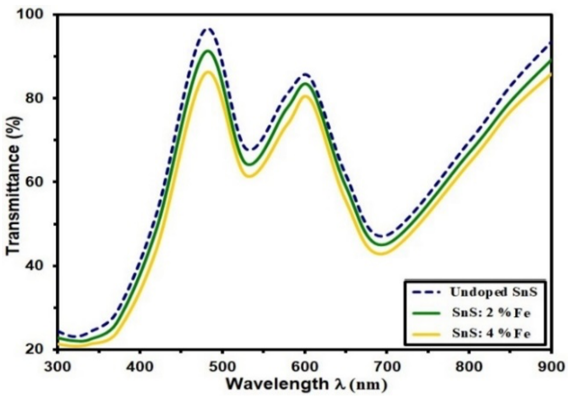

Figure 4: Optical transmittance spectra of pure and Fe-doped SnS thin films.

The optical band gap values obtained from the absorption spectra are presented in Figure 7. The band gap gradually decreases from 1.72 eV for the undoped SnS film to 1.60 eV for the film with the highest Fe concentration. This reduction is attributed to the formation of Fe-induced defect states within the forbidden energy gap, which introduce additional electronic levels between the valence and conduction bands. Furthermore, the increased structural disorder associated with Fe incorporation contributes to the observed band-gap narrowing [44]–[46].

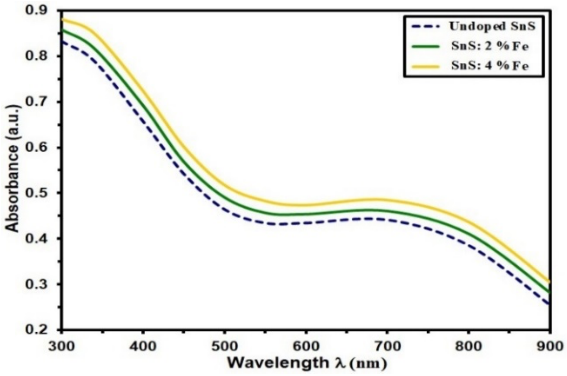

Figure 5: Absorption of SnS pure and SnS: Fe film.

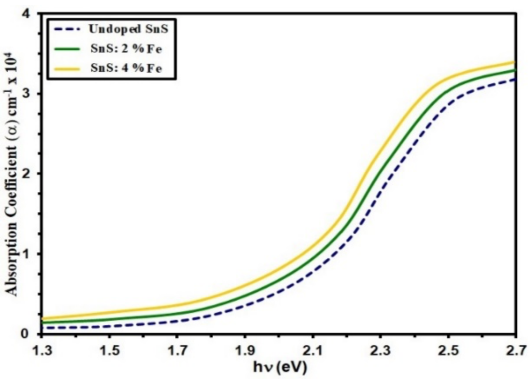

Figure 6: Absorption coefficient spectra of pure and Fe-doped SnS thin films.

Figure 8 shows the extinction coefficient spectra of the pure and Fe-doped SnS thin films. The extinction coefficient increases rapidly in the ultraviolet region and then gradually decreases with increasing wavelength. The non-zero extinction coefficient below the fundamental absorption edge indicates that part of the optical absorption originates from structural defects and impurity states introduced into the films [47], [48].

The wavelength dependence of the refractive index is presented in Figure 9. The refractive index decreases with increasing Fe concentration over the investigated spectral range. This behavior can be attributed to changes in the electronic polarizability and structural modifications induced by Fe incorporation, which alter the optical response of the SnS thin films [49]–[57].

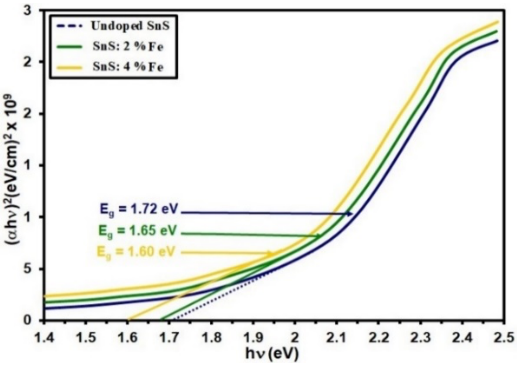

Figure 7: Optical band-gap plots of pure and Fe-doped SnS thin films.

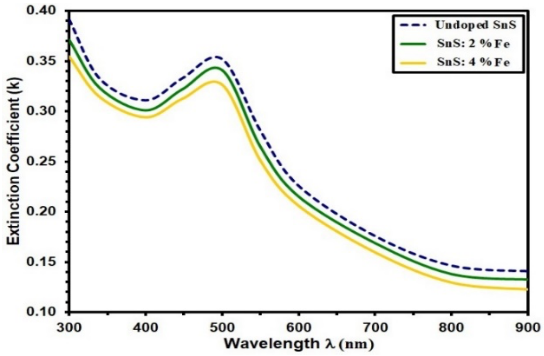

Figure 8: Extinction coefficient spectra of pure and Fe-doped SnS thin films.

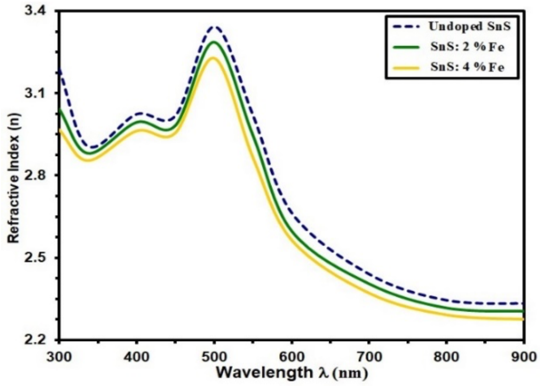

Figure 9: Refractive index spectra of pure and Fe-doped SnS thin films.

The gas-sensing performance of the fabricated films was evaluated at an operating temperature of 110 °C using NO_2 concentrations of up to 300 ppm. Figure 10 shows the variation in electrical resistance upon gas exposure. The undoped SnS film exhibits the lowest resistance, indicating more effective adsorption of NO_2 molecules on its surface [58]–[62]. In contrast, the Fe-doped films show progressively higher resistance with increasing Fe concentration, reaching the highest value for the 4% Fe-doped sample. This behavior is attributed to Fe-induced modifications of the charge-transport mechanism and the interaction between the sensing surface and NO_2 molecules, which reduce charge-carrier mobility and consequently increase the electrical resistance [62]–[65].

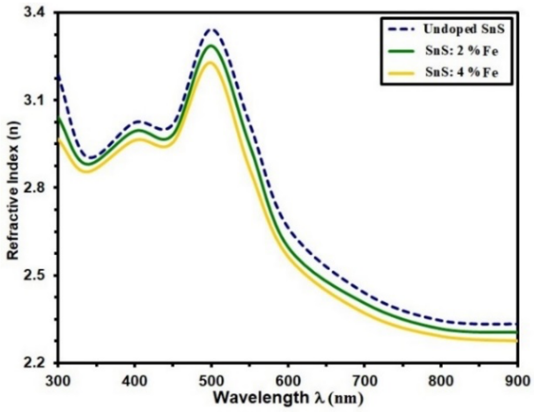

Figure 10: Dynamic resistance response of pure and Fe-doped SnS thin films toward NO_2 gas.

Figure 11 illustrates the NO_2 gas-sensing sensitivity of the pure and Fe-doped SnS thin films. The sensitivity decreases systematically with increasing Fe concentration over the investigated gas concentrations [66]–[68]. Specifically, the sensitivity decreases from 47.06% to 19.13% at 100 ppm, from 49.25% to 20.72% at 200 ppm, and from 53.02% to 22.33% at 300 ppm as the Fe content increases. This reduction is attributed to enhanced charge-carrier recombination and changes in the electronic structure caused by Fe incorporation, which reduce the number of free carriers participating in gas detection and consequently weaken the sensor response [69], [70].

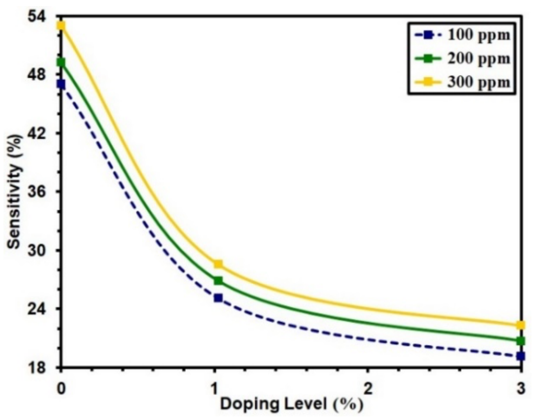

Figure 11: Sensitivity of undoped SnS and Fe content at 1% and 3% respectively.

4 CONCLUSIONS

This research successfully prepared SnS thin films with varying Fe doping levels of 1% and 3% via SPT. XRD assure that all films are polycrystalline with an orthorhombic structure and a dominant (106) preferred orientation. Fe doping significantly improved crystalline quality, increasing the crystallite size from 13.56 to 22.78 nm. This enhancement was accompanied by a notable reduction in both dislocation density (from 64.61×10^{14} to 50.60×10^{14} lines/m²) and microstrain, indicating a decrease in crystal lattice defects. Morphological studies using AFM revealed that Fe doping leads to smoother films with a finer nanostructure, as the average particle size decreased substantially from 87.6 nm to 41.1 nm. Optically, the films became more absorbent in the visible region with increasing Fe content, which correlated with a narrowing of the direct optical bandgap from 1.72 eV to 1.60 eV. Critically, the evaluation of NO_2 gas sensing properties at 110°C showed that Fe doping was detrimental to sensor performance. The sensitivity of the films decreased progressively with increasing Fe concentration, from 53.02% for the undoped film to 22.33% for the 3% Fe-doped film at 300 ppm NO_2.

ACKNOWLEDGMENTS

This work was upheld by Mustansiriyah University (www. uomustansiriyah.edu.iq).

REFERENCES

[1] S. Hasan, M. J. H. Kadhim, A. Hashim, A. E. Jassem, M. A. Al-shujairi, and Z. A. Kadem, "Exploring the electronic, structural and optical features of SiS2-LiF and SnS-SiBr4 new nanostructures doped PANI for optoelectronics and solar cells applications," Journal of Umm Al-Qura University for Applied Sciences, pp. 1-13, 2025.

[2] M. I. Afzal Basha and S. R. Meher, "Ab initio investigations on the effect of pressure on the structural, electronic, optical and vibrational properties of SnS," Physica Scripta, vol. 100, no. 3, 035969, 2025.

[3] M. Louhichi, R. Souissi, A. Alaya, M. Toumi, B. Tiss, A. B. H. Amara, … and S. Alaya, "Spray-pyrolyzed tin disulfide (SnS2) thin film: a promising approach for both visible and UV detection applications," Journal of Electronic Materials, vol. 54, no. 7, pp. 5709-5722, 2025.

[4] M. Balali-Mood, N. Eizadi-Mood, H. Hassanian-Moghaddam, L. Etemad, M. Moshiri, M. Vahabzadeh, and M. Sadeghi, "Recent advances in the clinical management of intoxication by five heavy metals: Mercury, lead, chromium, cadmium and arsenic," Heliyon, vol. 11, no. 4, 2025.

[5] H. Abdelmonem, L. T. Kamal, R. M. Elbaz, M. R. Khalifa, and A. Abdelnaser, "From contamination to detection: The growing threat of heavy metals," Heliyon, vol. 11, no. 1, 2025.

[6] V. Talapatadur, S. S. Hegde, N. Basavaraju, and K. Ramesh, "Solvothermal method synthesized SnS nanoplates composites for electrochemical sensing of toxic ions Hg2+ and Pb2+," Journal of the Iranian Chemical Society, vol. 22, no. 1, pp. 231-242, 2025.

[7] Liu, J. Hu, Z. Zhao, L. Yang, C. Su, N. Yan, and L. Liu, "Tuning the electronic structure of SnS for efficient inactivation of E. coli relying on defect engineering," Chemical Engineering Journal, 173120, 2026.

[8] M. Ijaz, K. S. Ahmad, J. S. Al-Hawadi, B. Makawana, R. K. Gupta, M. Alhabradi, … and A. BaQais, "Metal sulfides complex Sb2S3:SnS2:Cu1.95S (DDTC), exploring its synergistic effects on eco-friendly electrochemical energy employed in supercapacitors and electro-catalysis," Materials Science and Engineering: B, vol. 325, 119071, 2026.

[9] P. Sutter, A. Barinov, H. P. Komsa, P. Ghimire, L. Wu, Y. Zhu, … and E. Sutter, "SnSe1-xSx Alloys: Anisotropic Van der Waals Semiconductors with Tunable Bandgaps," Small, vol. 22, no. 4, e08578, 2026.

[10] F. Ayala-Mató, L. A. López-Cruz, E. Barrios-Salgado, M. T. S. Nair, and P. K. Nair, "Chemically deposited cubic/orthorhombic SnS superstrate solar cells with ZnS-CdS window and copper selenide back interface layers," Journal of Alloys and Compounds, 186107, 2026.

[11] S. Di Mare, D. Menossi, A. Salavei, E. Artegiani, F. Piccinelli, A. Kumar, … and A. Romeo, "SnS thin film solar cells: perspectives and limitations," Coatings, vol. 7, no. 2, p. 34, 2017.

[12] F. Baig, H. Ullah, Y. H. Khattak, and B. M. Soucase, "Numerical analysis of SnS Photovoltaic cells," in 2016 International Renewable and Sustainable Energy Conference (IRSEC), pp. 596-600, IEEE, 2016.

[13] Alagarasan, S. S. Hegde, S. Varadharajaperumal, R. Aadhavan, R. Naik, M. Shkir, … and R. Ganesan, "Effect of SnS thin film thickness on visible light photo detection," Physica Scripta, vol. 97, no. 6, 065814, 2022.

[14] X. Guo, F. Zhang, Y. Zhang, and J. Hu, "Review on the advancement of SnS2 in photocatalysis," Journal of Materials Chemistry A, vol. 11, no. 14, pp. 7331-7343, 2023.

[15] Motai, I. Suzuki, T. Nogami, and T. Omata, "Reactive sputtering of SnS thin films using sulfur plasma and a metallic Tin target: achieving stoichiometry and large grains," Scientific Reports, vol. 15, no. 1, 28917, 2025.

[16] D. B. Sánchez, M. T. S. Nair, and P. K. Nair, "Insights to the production of SnS-cubic thin films by vacuum thermal evaporation for photovoltaics," Semiconductor Science and Technology, vol. 39, no. 1, 015003, 2024.

[17] D. Motai, R. Ohashi, and H. Araki, "Effect of annealing temperature on p-n junction formation in Cu2SnS3 thin-film solar cells fabricated via the co-evaporation of elemental precursors," Japanese Journal of Applied Physics, vol. 61, no. SB, SB1043, 2022.

[18] S. Ildan Ozmen, S. H. Temiz, and H. M. Gubur, "Effects of annealing on SnS films produced by chemical bath deposition (CBD)," Physica Scripta, vol. 97, no. 7, 075704, 2022.

[19] X. Xu, X. Bai, T. Han, W. Dong, Y. Zhang, Y. Wang, and D. Hua, "High performance UV-Vis photodetectors based on tin monosulfide film synthesized by physical vapor deposition," Applied Surface Science, vol. 597, 153691, 2022.

[20] I. Gunes, "Enhancing π-SnS thin films and fabrication of p-SnS/n-Si heterostructures through flow rate control in ultrasonic spray pyrolysis for improved photovoltaic performance," Applied Physics A, vol. 130, no. 8, p. 574, 2024.

[21] P. Bisht, B. D. Belle, P. Aggarwal, A. Ghosh, W. Xing, N. Kaur, … and B. R. Mehta, "Gas sensing properties of PLD grown 2D SnS film: Effect of film thickness, metal nanoparticle decoration, and in situ KPFM investigation," Small, vol. 20, no. 23, 2307037, 2024.

[22] B. Lemli, S. Pál, A. Salem, and A. Szechenyi, "Prioritizing computational cocrystal prediction methods for experimental researchers: a review to find efficient, cost-effective, and user-friendly approaches," International Journal of Molecular Sciences, vol. 25, no. 22, 12045, 2024.

[23] T. Long, M. Wan, W. Jian, H. Dai, W. Nie, and J. Xu, "Application of multi-task transfer learning: The combination of EA and optimized subband regularized CSP to classification of 8-channel EEG signals with small dataset," Frontiers in Human Neuroscience, vol. 17, 1143027, 2023.

[24] B. Tatar and D. Demiroğlu, "The effect of depositions parameters on the nanostructural and optical properties of CuPc organic thin films growth by oblique angle deposition CSP technique," Physica Scripta, vol. 98, no. 7, 075909, 2023.

[25] A. A. Aboud, Z. S. Matar, and M. Mohaseb, "Effect of different metallic doping elements on the physical properties of iron oxide thin films," Physica Scripta, vol. 99, no. 11, 115926, 2024.

[26] Javed and M. Bashir, "Controlled growth, structure and optical properties of Fe-doped cubic π-SnS thin films," Journal of Alloys and Compounds, vol. 759, pp. 14-21, 2018.

[27] A. Alharshan, A. M. Aboraia, M. A. Uosif, I. M. Sharaf, E. R. Shaaban, M. Saad, and M. M. Elsenety, "Optical band gap tuning, DFT understandings, and photocatalysis performance of ZnO nanoparticle-doped Fe compounds," Materials, vol. 16, no. 7, p. 2676, 2023.

[28] S. Piccinin, "The band structure and optical absorption of hematite (α-Fe2O3): a first-principles GW-BSE study," Physical Chemistry Chemical Physics, vol. 21, no. 6, pp. 2957-2967, 2019.

[29] X. Zhou, J. Shi, and C. Li, "Effect of metal doping on electronic structure and visible light absorption of SrTiO3 and NaTaO3 (Metal = Mn, Fe, and Co)," The Journal of Physical Chemistry C, vol. 115, no. 16, pp. 8305-8311, 2011.

[30] R. S. Ali, H. S. Rasheed, N. F. Habubi, and S. S. Chiad, "Synthesis and characterization of manganese-doped FeS2 thin films via chemical spray pyrolysis," Chalcogenide Letters, vol. 20, no. 1, pp. 63-72, 2023.

[31] Rodríguez-Hoyos, I. H. Salmón, and E. Fernández-Díaz, "Research on SNS and education: The state of the art and its challenges," Australasian Journal of Educational Technology, vol. 31, no. 1, 2015.

[32] S. S. Chiad, H. A. Noor, O. M. Abdulmunem, N. F. Habubi, M. Jadan, and J. S. Addasi, "Optical and structural performance of nanostructured Te thin films by (CSP) with various thicknesses," Journal of Ovonic Research, vol. 16, no. 1, pp. 35-40, 2020.

[33] J. Zimou, M. Oubakalla, N. Ait Labyad, Z. Barbouch, E. Laghchim, K. Fareh, … and M. Addou, "Impact of defects and oxygen vacancies on the microstructural, optical, and electrochemical properties of Fe-doped CeO2 nanostructured films for supercapacitor devices," Journal of Energy Storage, vol. 109, 115162, 2025.

[34] S. Tamuli, D. Mohanta, and F. Singh, "Exfoliated layered nanosheets of orthorhombic SnS, subjected to 90 MeV carbon ion irradiation," International Journal of Modern Physics B, vol. 39, no. 5, 2540045, 2025.

[35] S. S. Kumar, S. Valanarasu, R. R. Isaac, A. V. Juliet, V. Ganesh, and I. S. Yahia, "Improve the photodetector properties of SnS thin films via nebulizer spray pyrolysis (NSP) technique for UV sensor applications," Journal of Alloys and Compounds, vol. 1019, 179275, 2025.

[36] C. Yen, K. Y. Chen, M. M. Ahmed, C. H. Syu, Y. T. Liu, Y. C. Hsieh, … and Y. M. Tzou, "Photochemical oxidation of Cr(III) to Cr(VI) in the presence of Fe(III): Influence of Fe(III) concentration and UV wavelength," Journal of Hazardous Materials, vol. 485, 136852, 2025.

[37] M. A. Issa and K. A. Aadim, "Optical and structural characterization of ZnO:NiO nano composite prepared by pulsed laser deposition method," J. Opt., vol. 54, pp. 2357-2362, 2025.

[38] Cheng, L. Ye, A. Wei, G. Xu, Z. Cao, P. Zhu, and Y. Chen, "Constructing SnS/Fe2O3 heterostructure anchored on few-layered graphene as an ion-adsorption/diffusion enhancer for ultrafast and cycle-stable sodium storage," Chemical Engineering Journal, vol. 457, 141243, 2023.

[39] B. H. Baby, N. T. Shajan, D. P. Joseph, G. K. Varghese, and D. B. Mohan, "Phase stabilization of Fe doped SnS by solvothermal method and its structural, morphological and optoelectronic properties for photovoltaic applications," Solid State Communications, vol. 386, 115525, 2024.

[40] M. A. Issa and K. A. Aadim, "Study the structural and optical properties of Zinc Oxide prepared by pulse laser deposition," J. Opt., 2024.

[41] A. Algamal, H. Abedi, U. Gandhi, O. Benafan, M. Elahinia, and A. Qattawi, "Manufacturing, processing, applications, and advancements of Fe-based shape memory alloys," Journal of Alloys and Compounds, vol. 1010, 177068, 2025.

[42] S. Hassan, A. K. Elttayef, S. H. Mostafa, M. H. Salim, and S. S. Chiad, "Silver oxides nanoparticle in gas sensors applications," Journal of Materials Science: Materials in Electronics, vol. 30, no. 17, pp. 15943-15951, 2019.

[43] X. Guo, F. Zhang, Y. Zhang, and J. Hu, "Review on the advancement of SnS2 in photocatalysis," Journal of Materials Chemistry A, vol. 11, no. 14, pp. 7331-7343, 2023.

[44] S. K. Muhammad, E. S. Hassan, K. Y. Qader, K. H. Abass, S. S. Chiad, and N. F. Habubi, "Effect of vanadium on structure and morphology of SnO2 thin films," Nano Biomedicine and Engineering, vol. 12, no. 1, pp. 67-74, 2020.

[45] B. Parveen, M. Hassan, S. Riaz, S. Atiq, S. Naseem, M. Irfan, and M. F. Iqbal, "Investigation of physical properties of SnS: Fe diluted magnetic semiconductor nanoparticles for spintronic applications," Journal of Magnetism and Magnetic Materials, vol. 460, pp. 111-119, 2018.

[46] Zhao, X. Xiao, L. Yang, Z. Wang, S. Xu, and J. Liu, "Synergistical coupling Janus SnS-Fe1-xS heterostructure cell and polydopamine-derived S doped carbon as high-rate anodes for sodium-ion batteries," Chemical Engineering Journal, vol. 425, 130534, 2021.

[47] X. Gou, G. Wang, J. Yang, J. Parka, and D. Wexler, "Chemical synthesis, characterization and gas sensing performance of copper oxide nanoribbons," Journal of Materials Chemistry, vol. 18, no. 9, pp. 965-969, 2008.

[48] A. Alibi, N. Elleuch, S. Shova, J. Lhoste, G. Duval, and M. Boujelbene, "Comprehensive structural and DFT analysis of a newly synthesized bismuth-based organic-inorganic hybrid material: in-depth insights into vibrational, optical, and photoluminescence properties of (C8H14N2)2[Bi2Br10]·2H2O," RSC Advances, vol. 15, no. 48, pp. 40439-40455, 2025.

[49] D. M. Shaker, R. R. Ahmed, A. M. Mohammad, T. H. Mubarak, and I. H. Mohamed, "Synthesis and characterization of CoZnFe2O4 ferrite nanoparticles by co-precipitation method for biomedical applications," Passer Journal of Basic and Applied Sciences, vol. 6, no. 2, pp. 488-493, 2024.

[50] J. Navrátil, O. Caha, J. Kopeček, P. Čermák, J. Prokleška, V. Holý, and Č. Drašar, "Electronic properties of Fe impurities in SnS van der Waals crystals-Revealing high-mobility holes," Materials Science and Engineering: B, vol. 301, 117148, 2024.

[51] Z. K. Heiba, A. A. Ellatief, H. Elshimy, S. I. Ahmed, and M. B. Mohamed, "Impact of iron doping on the structural and optical properties of nano Tin mono-sulfide SnS," Optical and Quantum Electronics, vol. 56, no. 1, p. 42, 2024.

[52] L. Sun, D. Westerdahl, and Z. Ning, "Development and evaluation of a novel and cost-effective approach for low-cost NO2 sensor drift correction," Sensors, vol. 17, no. 8, p. 1916, 2017.

[53] N. Manh Hung, C. V. Nguyen, V. K. Arepalli, J. Kim, N. Duc Chinh, T. D. Nguyen, … and D. Kim, "Defect-induced gas-sensing properties of a flexible SnS sensor under UV illumination at room temperature," Sensors, vol. 20, no. 19, p. 5701, 2020.

[54] S. Al-Rikabi, M. H. Al-Timimi, and W. H. Albanda, "Morphological and optical properties of MgO1-xZnSx thin films," Digest Journal of Nanomaterials and Biostructures, vol. 17, no. 3, pp. 889-897, 2022.

[55] M. A. H. H. Mahmoud, A. M. El Sayed, and M. S. A. Abdel-Mottaleb, “Structural, optical, and electrical properties of SnS thin films deposited by chemical bath deposition: Effect of annealing temperature,” Thin Solid Films, vol. 750, 139212, 2022.

[56] P. K. Sahoo, R. Thangavel, and L. S. Panchakarla, “Emerging applications of SnS and SnS2 nanostructures in energy and environmental remediation,” ACS Applied Nano Materials, vol. 6, no. 15, pp. 13845-13870, 2023.

[57] K. S. Urmila, S. S. Patil, and R. R. Kharade, “Pulsed laser deposition of SnS thin films: Optimization of deposition parameters for photovoltaic applications,” Materials Today: Proceedings, vol. 72, pp. 312-318, 2023.

[58] S. N. F. M. Noor, S. A. M. Salleh, and M. H. M. Wahid, “Recent progress in SnS-based heterojunction photodetectors: A review,” Sensors and Actuators A: Physical, vol. 358, 114456, 2023.

[59] A. D. Patel, R. K. Patel, and N. M. Shah, “Doping strategies for improving the performance of SnS thin films for optoelectronic devices: A systematic review,” Materials Science in Semiconductor Processing, vol. 156, 107298, 2023.

[60] M. A. Issa and K. A. Aadim, “Spectroscopic analysis of plasma parameters for SnO2 doped ZnO prepared by pulse Nd:YAG laser deposition,” Journal of Physics: Conference Series, vol. 1795, no. 1, 012045, 2021.

[61] M. B. Jumaa, T. H. Mubarak, and A. M. Mohammad, “Synthesis and characterization of spinel ferrite Co0.8Fe2.2O4 nanoparticle,” Journal of University of Anbar for Pure Science, vol. 15, no. 2, pp. 74-82, 2021.

[62] S. S. Pawar, S. M. Mane, and S. R. Jadkar, “Recent advances in SnS thin film solar cells: A comprehensive review on fabrication strategies and performance enhancement,” Solar Energy, vol. 265, 112089, 2023.

[63] T. R. Lenka, S. K. Tripathy, and P. K. Sahu, “Numerical simulation of SnS-based heterojunction solar cells: Effect of absorber layer thickness and doping concentration,” Optical Materials, vol. 135, 113256, 2023.

[64] M. A. Rahman, S. M. Hossain, and A. K. M. A. Hossain, “Hydrothermal synthesis of Fe-doped SnS2 nanosheets for enhanced visible-light photocatalytic activity,” Materials Research Bulletin, vol. 168, 112487, 2023.

[65] L. Zhang, Y. Wang, and X. Chen, “Room-temperature NO2 gas sensors based on SnS nanostructures: A review of recent advances,” Sensors and Actuators B: Chemical, vol. 398, 134726, 2024.

[66] R. K. Mishra, S. K. Singh, and A. K. Srivastava, “Cr-doped SnS2 nanosheets for enhanced photocatalytic degradation of organic pollutants under visible light,” Journal of Environmental Chemical Engineering, vol. 10, no. 3, 107654, 2022.

[67] Y. S. Madansure, S. D. Balsure, P. K. Gaikwad, D. G. Mugale, K. M. Batoo, M. Hadi, and S. K. Gurav, “A detail investigation on the structural, elastic, magnetic and dielectric properties of rare earth Dy3+ substituted Fe rich cobalt ferrite nanoparticles,” Materials Chemistry and Physics, vol. 337, 130561, 2025.

[68] K. Mosupi, M. Masukume, G. Weng, N. M. Musyoka, and H. W. Langmi, “Recent advances in Fe-based metal-organic frameworks: Structural features, synthetic strategies and applications,” Coordination Chemistry Reviews, vol. 529, 216467, 2025.

[69] K. A. Aadim, “Spectroscopic study the plasma parameters for SnO2 doped ZnO prepared by pulse Nd:YAG laser deposition,” Iraqi Journal of Physics, vol. 17, no. 42, pp. 125-135, 2019.

[70] Y. G. Wang, Z. Jiao, and M. Zhong, “Density functional study of the structural, phonon, elastic and optical properties of hexagonal SnS2,” Physica B: Condensed Matter, vol. 714, 417462, 2025.